Detection of vaccinia virus proteins in wastewater environment using biofunctionalized optical fiber semi-distributed FBG-assisted interferometric probes

Sensing and Bio-Sensing Research 46 (2024) 100699

Contents lists available at ScienceDirect

Sensing and Bio-Sensing Research

journal homepage: www.elsevier.com/locate/sbsr

Detection of vaccinia virus proteins in wastewater environment using biofunctionalized optical fiber semi-distributed FBG-assisted interferometric probes

Albina Abdossova [a,1], Aina Adilzhankyzy [a,1], Kuanysh Seitkamal [b,c,1], Massimo Olivero [d], Guido Perrone [d], Wilfried Blanc [e], Luca Vangelista [f], Daniele Tosi [a,b,*]

[a] School of Engineering and Digital Sciences, Nazarbayev University, Astana, Kazakhstan
[b] Laboratory of Biosensors and Bioinstruments, National Laboratory Astana, Astana, Kazakhstan
[c] School of Medicine, Nazarbayev University, Astana, Kazakhstan
[d] Department of Electronics and Telecommunications, Politecnico di Torino, Turin, Italy
[e] Université Côte d'Azur, INPHYNI, CNRS UMR7010, 06200 Nice, France
[f] Department of Molecular Medicine, University of Pavia, 27100 Pavia, Italy

ARTICLE INFO

Keywords:
Optical fiber biosensors
Semi-distributed interferometer
Virus detection
Wastewater-based diagnostic
Surface functionalization
Vaccinia virus

ABSTRACT

In this work, we present the detection of proteins expressed by poxvirus with fiber-optic probes based on a semi-distributed interferometer (SDI) assisted by a fiber Bragg grating (FBG), performing the measurement directly into a wastewater sample. Modern biosafety applications benefit from real-time, dynamic-sensing technologies that can perform diagnostic tasks into a wide set of analytes, with a particular emphasis on wastewater, which appears to collect a significant number of viral titers in urban and indoor environments. The SDI/FBG probe can perform substantial progress in this field, as it embeds a dual sensitivity mechanism to refractive index changes (sensitivity up to 266.1 dB/RIU (refractive index units)) that can be exploited in biosensing, while simultaneously having the capability to measure the temperature (sensitivity 9.888 pm/°C), thus providing an intrinsic cross-sensitivity compensation. In addition, a standard FBG analyzer can be used as an interrogator, improving affordability and real-time detection over previous works. The probes have been functionalized with antibodies specific for L1, A27 and A33 vaccinia virus proteins, performing detection of a protein concentration in a scenario compatible with online viral threat detection. Direct detection of wastewater samples shows that the L1-functionalized sensor has a higher response, 9.1–11.3 times higher than A33 and A27, respectively, with a maximum response of up to 1.99 dB and excellent specificity. Dynamic detection in wastewater shows that the sensors have a response over multiple detection cycles, with a sensitivity of 0.024–0.153 dB for each 10-fold increase of concentration.

1. Introduction

The development of technologies for the rapid and accurate detection of viruses has been the subject of several studies over the last decade [1,2]. Then, the outbreak of SARS-CoV-2 pandemic in 2020 provided a framework for the development and testing of several diagnostic and preventive measurements [3], both from a purely biosensing perspective and in terms of internet-of-things (IoT) platforms, developed by several countries [4] and research institutions [5,6]. The short surge of Monkeypox recorded in 2022 [7] brought back attention to poxviruses, particularly to the deadly agent smallpox. Furthermore, the possibility of resurrecting horsepox by means of molecular biology [8] carries implications in the dual use of research [9].

Polymerase chain reaction (PCR) is currently the most popular method for the diagnostic of viral threats [10]; through the COVID-19 pandemic, PCR has been massively used as a test method for respiratory samples collected in nasal and mouth sites [11], with more recent works covering the possibility to use PCR in other liquid analytes [12]. However, due to the long sample processing time of PCR testing, this technique is effective for massive screening but lacks a real-time

* Corresponding author.
E-mail address: daniele.tosi@nu.edu.kz (D. Tosi).
[1] These authors contributed equally to the work.

https://doi.org/10.1016/j.sbsr.2024.100699
Received 24 June 2024; Received in revised form 4 October 2024; Accepted 22 October 2024
Available online 23 October 2024

response that would be beneficial for biosafety applications.

Label-free optical technologies that rely on functionalizing the dielectric substrate of an optical material with bioreceptors provide a faster detection method, as the viral particles could bind to the sensing location and provide a direct response in the transmission of the reflection spectrum. Such technologies can be implemented through surface plasmon resonance [13], lossy mode resonance [14], Raman scattering [15], or optical fiber biosensors (OFBSs) [16].

In terms of biosafety, optical fiber biosensing systems provide significant advantages over the other technologies [17]. At first, OFBSs can be multiplexed into a large network of sensors, using not only time/wavelength-division multiplexing approaches [18] but also other more advanced methods derived from distributed sensing [19]. Then, since single-mode fibers (SMFs) used in telecommunications have the lowest attenuation among transmission lines (0.18 dB/km), it is possible to remote the analyzer (i.e., the sensor interrogating system that includes the light source and detectors) with respect to the sensor. This remote placement of the analyzer is common in oil and gas [20] and aviation industries [21]. In the applications considered in this paper, OFBSs might enable the detection of viral agents in outdoor scenarios, for example interrogating wastewater collected in an urban environment [22], or for indoor use, for example detecting in gray water tanks on board of airplanes [23]. Another advantage is the small size of sensors, which enables micro-size packaging and integration into the environment, ideal for medical devices; moreover, combined with the possibility to handle very small sample sizes [24].

In this work, we demonstrate the possibility of deploying a network of optical fiber sensors to detect poxvirus proteins in wastewater samples, with each biosensor functionalized for a specific protein and analyzed by the real-time interrogator. The real-time detection in a wastewater sample collected and updated after each step is the enabling point for the online, IoT-compatible detection of viral agents in a scenario compatible with urban or indoor deployment. The sensors used in these experiments consist of semi-distributed interferometers (SDIs) [25,26] assisted by a Fiber Bragg Grating (FBG) for the measurement of temperature [27].

The case scenario developed in this work involves a network of fiber-optic sensors, each with distinct biofunctionalization, for real-time detection of poxvirus [28]. The detection is performed with a standard dynamic and multi-channel analyzer for FBG sensors (up to 16 channels for commercial FBG analyzers, possibly extended to hundreds using switches or other multiplexing protocols [18]). As the sensors operate at ambient temperature, it is necessary to measure the actual temperature and compensate for thermal variations. All interconnects are performed with SMF fibers, which have a maximum two-way loss of 0.4 dB/km; with the use of conventional FBG analyzers and the SDI sensors presented in this work, the power budget is sufficient for over 15 km of fiber spans, even in presence of splitters, satisfying the remote sensing scenario. SDI sensors have an extremely simple splice-and-cleave fabrication [26], leading to an estimated bill-of-material cost <1 USD; this means that the SDI sensors can be replaced after each detection or after the functionalization layers wear out, while the FBG used for temperature sensing (based on a fiber without any overlay), which may more complicated, thus expensive to fabricate, does not need any replacement.

The system tested in this work is designed to be seamlessly integrated, as shown in Fig. 1, in a sensing network designed for viral agent detection in liquid media. Wastewater has been selected as a viable matrix for the analysis of potential viral outbreaks, with pivotal works being carried out in the late 1990s [29] on static wastewater samples. The COVID-19 pandemic however shifted the technological paradigm to online detection. This type of design was first envisioned by Barcelo [30], drawing attention to online, IoT-compatible detection methods for epidemiologic platforms, and by Daughton [31], who focused on sample preparations for pathogen detection. The experimental proof of concept reported by Wu et al. [32] showed an increase in SARS-CoV-2 viral titers

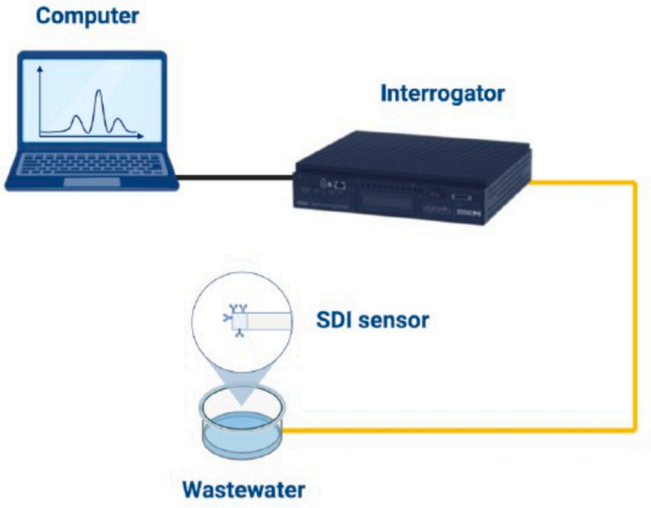

Fig. 1. Schematic of the system.

recorded in the wastewater up to 3 orders of magnitude between pre-pandemic samples and the peak of diagnosed COVID-19 patients.

The first step towards the detection of smallpox using optical fiber sensors was reported by Seitkamal et al. [28] using ball resonator sensors assisted by a tilted FBG. In this work, the detection of three ectodomains having antigenic importance (L1, A27, A33) was carried out using sensors, each biofunctionalized with antibodies binding to the protein under analysis. The results of the analysis, performed over a wide range of protein concentrations (15 aM to 1 μM), showed a log-quadratic performance in a simple medium such as phosphate buffer saline (PBS), and a log-linear metric with normalized sensitivity of 3.83 $\times$ 10^{-3} to 1.380 $\times$ 10^{-2} RIU (refractive index units) for each 10-fold protein increment when the protein was diluted in a complex matrix such as fetal bovine serum (FBS).

A subsequent study reported by Rakhimbekova et al. [33] showed how ball resonator sensors undergoing the same biofunctionalization process could detect the vaccinia virus, which presents proteins highly homologous to those of smallpox. This study showed that a ball resonator biosensor functionalized with anti-L1 antibodies binds to the viral particle and expresses a log-quadratic pattern, similar to protein biosensing in the same medium [34]. Thus, the fiber-optic biosensor functionalized with a protein-binding bioreceptor can also detect the whole viral particle with a similar trend. The recorded sensitivity was 1.081 $\times$ 10^{-2} to 1.246 $\times$ 10^{-2} RIU for each 10-fold increment of viral concentrations from 10^4 to 10^8 PFU (plaque-forming units). The behavior of the sensors in the protein detection scenario shows substantial analogies with the detection of viral particles with sub-wavelength size (~250–360 nm [35]). In this work, carrying on the analogy between the protein ectodomain and the viral particle, we show the behavior and performances of the detection in wastewater, using the L1, A27, and A33 proteins dissolved in wastewater samples at various concentrations, mimicking the sample sequential collection proposed in another work [31].

2. Materials and methods

2.1. Chemicals

1× Phosphate-Buffered Saline, 0.1 % Tween® 20 Detergent (PBST) (Thermo Scientific Chemicals), peptone (Thermo Scientific Chemicals), Beef Extract Powder (Fluka Analytical), ammonium chloride (≥99 %) (TCI chemicals), Bovine serum albumin sodium chloride (≥99 %), sucrose, hydrogen peroxide, sulfuric acid, 3-Aminopropyl trimethoxysilane (APTMS), methanol, glucose monohydrate, Glutaraldehyde

solution, anhydrous potassium monohydrogen phosphate (≥98 %), disodium hydrogen- phosphate dehydrate (≥98 %), sodium hydrogen carbonate (≥98 %), iron (III) chloride hexahydrate (≥99 %) were purchased from Sigma-Aldrich (Germany).

2.2. Preparation of recombinant vaccinia virus proteins and dot blot assay

Recombinant vaccinia virus proteins were prepared using the pET23a expression vector system, as previously described [28]. Monoclonal anti-vaccinia virus (WR) antibodies targeting L1R (residues 1 to 185), A33R (residues 58 to 18), and A27L (residues 1 to 110), were obtained from the NIH Biodefense and Emerging Infections Research Resources Repository (BEI Resources). To determine the specificity of the antibodies to the antigens, a dot blot assay was conducted. Briefly, 10 μl of the antigen (recombinant vaccinia virus protein) was spotted onto a nitrocellulose membrane (NCM). The NCMs were air-dried and subsequently blocked in 5 % skimmed milk/TBST, pH 7.4, for 2 h. After washing three times with TBST, the membrane was incubated with the anti-vaccinia virus monoclonal antibody (diluted at 1:2000) for 1 h. After washing, the membranes were revealed with Goat Anti-Rabbit IgG secondary antibody (Sigma-Aldrich, St. Louis, Missouri, USA). Color development was achieved using SuperSignal™ West Pico PLUS Chemiluminescent Substrate (BioRad). The density of the blots was quantified utilizing the ChemiDoc MP Imaging system (BioRad).

2.3. Wastewater sample preparation

The recombinant vaccinia proteins underwent serial dilution in wastewater prepared within our laboratory. The formulation of synthetic municipal wastewater was derived from the ISO11733 Standard [36]. Details regarding its composition are outlined in Table 1.

2.4. Fabrication of the sensors

The process of fabrication of the SDI sensor requires two types of fibers: an enhanced backscattering fiber (EBF) that acts as a reflector and a standard single-mode fiber (SMF; Corning SMF- 28). Enhanced backscattering fibers (EBFs) have significantly higher scattering content which was achieved using fibers doped with MgO-based nanoparticles (MgO-NP) within the core, which can be handled like standard fibers. The advantage of EBFs over standard fibers extends beyond improving the signal-to-noise ratio. With a proper arrangement, they can generate a new multiplexing domain called scattering-level multiplexing (SLMux), enabling the simultaneous detection of multiple fibers [37].

The sensors were developed through a splice and cleave approach that requires simple manual handling with telecom-grade fusion splicing equipment. Initially, the fibers were spliced together using a standard telecom splicer (Fujikura 12-S, SMF-SMF recipe) so that the cores of both fibers were perfectly matched. Due to the presence of scattering centers, the interface between the SMF and the EBF provides a tiny reflectivity ($\sim 10^{-5}$). After that, a cavity was formed manually by cleaving the EBF fiber at a very short distance of less than 1 mm using a fiber cleaver (Fujikura CT-08), forming a tip mirror. The schematic view of the fabrication process is shown in Fig. 2.

Table 1
Synthetic wastewater composition.

Content	Concentration, mg/L
Peptone	192
Beef Extract Powder	138
Glucose monohydrate	19
Ammonium chloride (NH4Cl)	23
Potassium dihydrogen phosphate (K2HPO4)	16
Disodium hydrogen phosphate dihydrate (Na2HPO4x2H2O)	32
Sodium hydrogen carbonate (NaHCO3)	294
Sodium chloride (NaCl)	60
Iron (III) chloride hexahydrate (FeCl3x6H2O)	4

The SDI sensors were complemented with fiber Bragg grating (FBG) sensors to allow the simultaneous measurement of the temperature, and thus to compensate for cross-sensitivity effects. FBGs are quite common fiber optic temperature sensors in biomedical applications [38,39] and have been fabricated by inscription in the fiber core of a standard SMF using a femtosecond laser [40]. The electromagnetic model of the SDI sensor used in this work can be found in [25], including a software designed in Matlab for the generation of SDI spectra; in Suppl. Mat., we list the parameters to use for this code in order to match the shape of the spectra reported in this work, and some additional spectra of SDI/FBG sensors.

2.5. Sensor interrogation

The experimental setup used for the calibration and measurements is shown in Fig. 3. The interrogation of the SDI/FBG probes was performed using a dynamic FBG interrogator (Micron Optics si255, VA, US), using the spectral scanning mode. The interrogator includes a swept laser with an array of photodetectors, with each channel physically split. Up to 5 channels were used for simultaneous detection, each using an SDI/FBG probe. Data analysis was carried out in MATLAB® (MathWorks, US). Spectral data have been processed first by a digital low-pass filter (Butterworth, 5th order, cut-off 0.01), then by separating the FBG spectrum from the SDI spectral comb. The FBG spectral shift has been estimated using a spline wavelength fitting method [18]. The refractive index (RI) dependence and the biological measurements have been performed by tracking every peak/valley in the SDI spectrum, having prominence ≥1 dB.

2.6. Refractive index and thermal calibration

All sensors used in the experiments have been calibrated for refractive index analysis, using 6 sucrose mixtures covering an RI span of 0.01084 RIU, from 1.34761 to 1.35845. The RI values have been referenced using an Abbe refractometer. Temperature calibration was conducted using a water bath, using a reference sensor (IKA Thermocouple), operating from 27 °C to 61 °C in steps of approximately 4 °C.

2.7. Surface biofunctionalization

The process of biofunctionalization, as depicted in Fig. 4 and described below, involved several steps. The SDI surface was cleaned by immersing it in a piranha solution comprising a mixture of sulfuric acid and hydrogen peroxide in a 4:1 ratio. This step was conducted for 15 min at room temperature to activate the sensor's surface and ensure the effective elimination of organic contaminants. Following this, the surface was rinsed with deionized (DI) water and dried using nitrogen gas. The cleaned optical fibers were treated with a solution containing 1 % (3-aminopropyl)trimethoxysilane (APTMS) in methanol for 30 min at room temperature for further silanization. The region treated with APTMS is then rinsed with methanol and placed in an oven at 110 °C for 1-h heat treatment. Subsequently, the silanized SDI sensors were incubated in a glutaraldehyde solution (25 % in PBS) for 1 h and washed with PBS. The fibers were then incubated overnight in a 500 μL solution containing 8 μg/mL of anti-vaccinia antibodies for 3 h under continuous shaking. The unreacted aldehyde groups were then blocked with 1 % BSA for a duration of 1 h and subjected to another round of PBS rinsing before being utilized for protein detection.

2.8. Virus protein measurement

To perform protein measurement with functionalized sensors, serial dilution of mixed L1, A33, and A27 recombinant virus proteins with concentrations ranging from 2.5 fM to 400 nM in artificial municipal wastewater was prepared. By connecting the sensor to the dynamic FBG

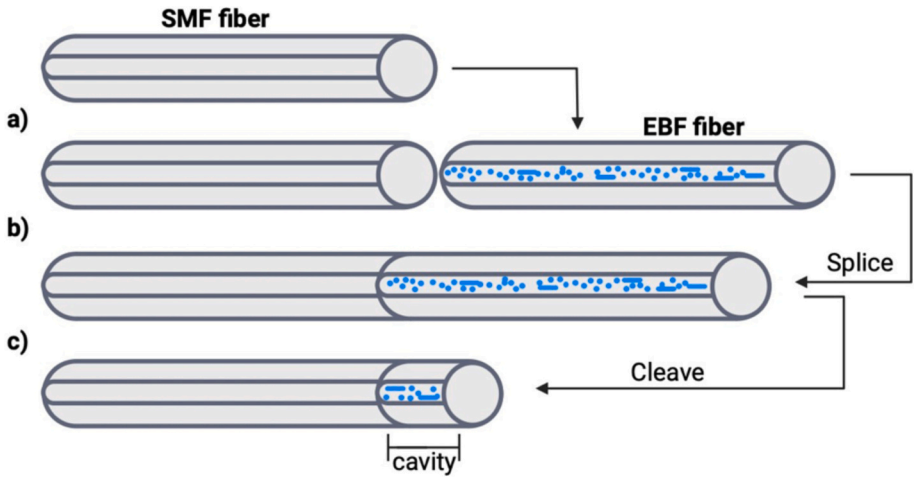

Fig. 2. Overview of the sensor fabrication and interrogation of the SDI interferometer for RI sensing, highlighting the splice-and-cleave operation: a) an EBF is spliced to a standard SMF; b) the EBF is manually cleaved; c) a cavity is formed between tip and SMF/EBF mirrors.

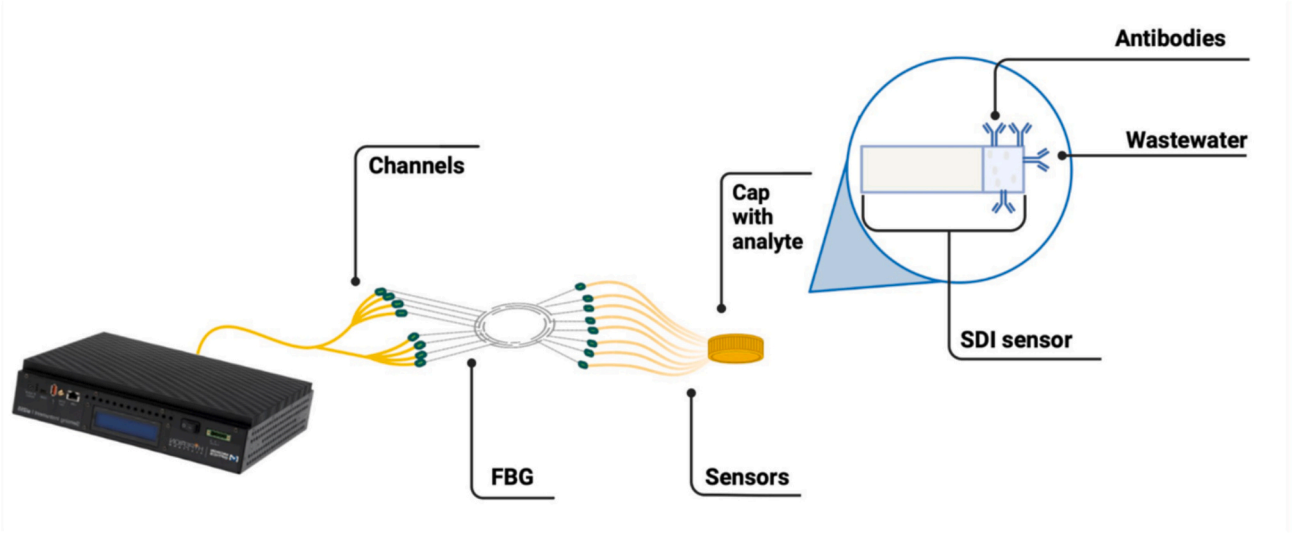

Fig. 3. Setup for measurement of vaccinia virus proteins in wastewater.

interrogator device and placing the tip of the sensor in the vial with 200 μL of protein solution, measurements were performed starting from the artificial wastewater as a blank solution. The position of the sensor within the vial and overall setup can be seen in Fig. 3. For each protein concentration, 25 measurements were performed, with an interval of 1 min. The signal was recorded under stable, quiet, room temperature conditions, to prevent any disturbances in measurement.

3. Results

3.1. Operation of the SDI/FBG biosensor

The refractive index capability and the spectral behavior of an SDI/FBG probe are displayed in Fig. 5. The spectrum of the probe combines the spectral features of the SDI, which appears as a broadband interferometer with a fluctuating envelope due to the random distribution of the scattering centers within the cavity, and the FBG, which appears as a thin spectral line at 1551 nm. As shown in Fig. 5(a-c), the RI changes are encoded in the variations of the intensity of the spectral peaks and valleys, each recording a reduction in the intensity due to the lower Fresnel reflection at the fiber tip. Conversely, the FBG spectrum appears unchanged, as expected since gratings written in fiber core do not show any detectable sensitivity to the surrounding RI. In order to perform a detection across the whole spectrum, all peaks and valleys have been localized using a peak tracking method [18], which detects all features having significant prominence and free spectral range. Then, the sensitivity can be estimated in each peak or valley, as shown in Supplementary Fig. S1, obtaining the trace shown in Fig. 5(e). This sensor shows a sensitivity higher in the spectral valleys, as shown in previous works [25]. For spectral valleys, the sensitivity achieves a maximum value of 266.10 dB/RIU, with an average value of 183.97 dB/RIU and a standard deviation of 33.92 dB/RIU. The spectral peaks have lower sensitivity, with a maximum of 166.50 dB/RIU and an average of 106.17 dB/RIU and a standard deviation of 27.03 dB/RIU. All the spectral features shown in this chart exhibit a coefficient of determination $R^2 > 0.95$. As the analyzer has a noise floor estimated in 0.02 dB, the RI detection accuracy is $\sim 10^{-4}$ RIU, which is compatible with accurate biosensing. We report in Supplementary Table S1 the RI values for all the SDI/FBG sensors used in the experiments reported for protein sensing.

The temperature sensing capability, necessary for real-time operation in environmental scenarios [41], is shown in Fig. 6 for a sensing probe. The reflection spectra appear to shift towards a longer wavelength when a temperature increment is recorded; as shown in the insets (b-d), this occurs both for the FBG and for each spectral feature localized

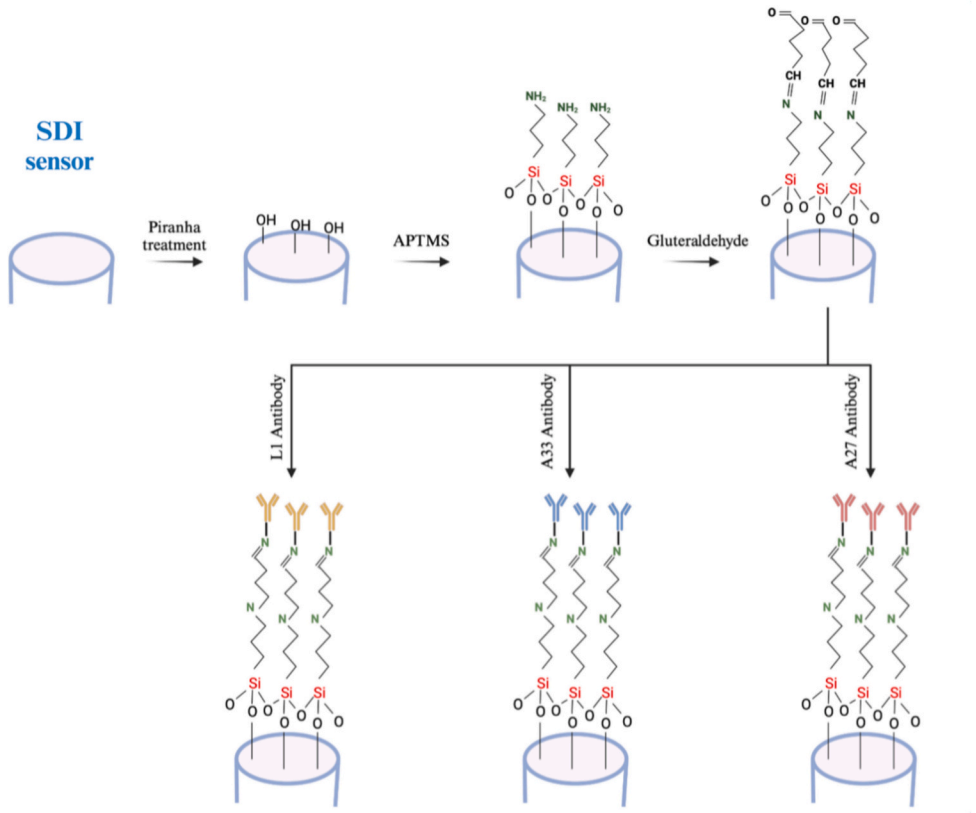

Fig. 4. The process of biofunctionalization of the sensor with vaccinia virus antibodies.

within the SDI. The wavelength shift estimated for the FBG is 9.888 pm/°C, very close to that of shown by any grating in standard telecom fibers [42]; similarly, the temperature effect can be estimated for the interferometer as shown in Supplementary Fig. S2. For the SDI, the wavelength shift appears to be lower, ranging from 4.267 pm/°C to 9.177 pm/°C for spectral peaks and from 4.268 pm/°C to 9.391 pm/°C for spectral valleys; the median values, as shown in Fig. 6 (g), are 6.004 pm/°C and 7.232 pm/°C, respectively.

3.2. Direct detection in wastewater

The first biological experiment was carried out to demonstrate the direct detection capability, where the sensor is exposed to various and increasing concentrations of the vaccinia virus proteins, and verifying the response and detection limits; the results are shown in Fig. 7, while the spectral sensorgram for each spectral feature is shown in Supplementary Fig. S3.

We observe that the spectrum of the SDI/FBG probe follows the pattern observed in the RI calibration; each of the spectral peak/valley in the spectrum responds to the biological changes according to the biofunctionalization process, while the FBG remains unchanged during the whole measurement as the environmental temperature is controlled to <1 °C variations. The analysis of the spectral portions shows that, even at low concentrations, the changes from the reference condition are well detectable; however, the pattern appears to vary for each peak/valley. The sensorgram for each spectral valley, reported in Fig. 7(e), shows that for each incremental change of protein concentration, we observe a detectable shift in the spectral pattern, although this is not always consistent between the spectral features. By selecting the most responsive feature, which corresponds to the spectral dip at 1596.7 nm, we can estimate the response of the sensor as reported in Fig. 7(f). In wastewater, the sensor appears to have good stability, with a standard deviation of ±0.15 dB over 10 consecutive samples. At the lowest protein concentration of 2.5 fM, we observe a response of −0.17 dB, which is well detectable by the interrogator. The average response is then −0.67 dB for 50 pM, −1.79 dB for 1 nM, −1.99 dB for 20 nM, and finally −1.57 dB for 400 nM, while the maximum standard deviation is ±0.52 dB. While the response appears to be well detectable even at the lowest concentrations, the overall pattern displays a concentration-dependent trend that is less linear and consistent than the previous works reported in PBS buffer and in serum [28], and this can be attributed to the influence of the wastewater medium. We can draw an approximate response slope of −0.268 dB for each 10-fold protein concentration increase (R^2 = 0.76), which can lead to an analytical detection limit of 1.4 nM using the $y_{blank} + 3\sigma_{max}$ threshold (y_{blank} = blank sample level; σ_{max} = maximum standard deviation); however, the experimental data show that even changes below the nanomolar level are well detected by the L1-functionalized biosensor. With the signal processing done in this analysis, the FBG interrogator can detect at a resolution of 0.01–0.02 dB, which suggests that the accuracy in the detection is largely dependent upon the wastewater sample handling, possibly to be improved using filtering methods [30,32].

The observed sensitivity for protein detection is compatible with other sensors detecting intensity changes, and using a similar biofunctionalization: among others, Bekmurzayeva et al. reported cancer biomarker detection with a ball resonator with sensitivity 0.091 dB per 10-fold increase [34] while Rakhimbekova et al. reported a sensitivity of 0.218 dB per 10-fold increase [26] both in serum and with silanized sensors. Gold-coated version of this sensors have shown higher biological sensitivity, such as 1.64 dB per 10-fold increase reported by Sypabekova et al. [43] and 1.23 dB per 10-fold increase reported by Bekmurzayeva et al. [44].

In order to validate the effect of the antibodies and obtain insights into the efficiency of the biofunctionalization process, we compared the response of three different sensors fabricated with the same method, and functionalized with L1 (same sensor shown in Fig. 7), A27, and A33

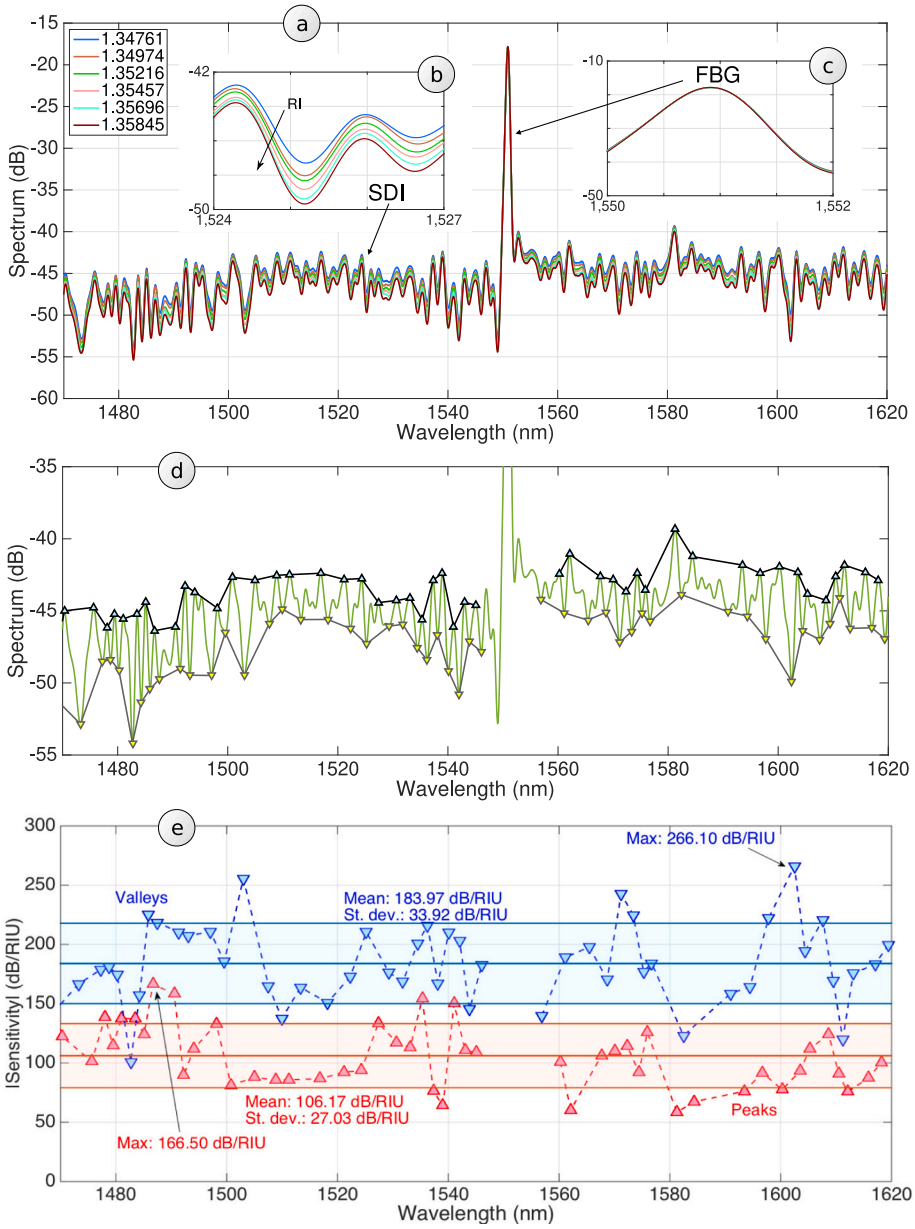

Fig. 5. Refractive index sensitivity of the SDI/FBG probe. (a) The spectrum of the probe for different values of RI; insets show the spectral features corresponding to (b) a portion of the SDI spectrum, and (c) the FBG spectrum. (d) Localization of the spectral peaks and valleys in the SDI spectrum. (e) Evaluation of the RI sensitivity for each spectral feature.

antibody, and in addition a negative control functionalized without antibodies. All sensors tracked the same concentration increase from the reference wastewater sample, up to 400 nM protein concentration. The results are shown in Fig. 8, which compares the response (i.e. the decrease of intensity from the reference condition) for all sensors.

We observe that the direct detection with the L1-functionalized sensor yields the highest response (up to 1.99 dB), while the A33 sensor has a response of up to 0.28 dB and the A27 probe has a maximum response of 0.17 dB. At the largest concentration, the response of the L1 sensor is 11.3 times higher than the A33 probe, and 9.1 times higher than the A27 sensor. We can also observe that the measurement has a substantial specificity, as the negative control sensor has a maximum intensity of 0.02 dB, and therefore negligible with respect to the other sensors. A specificity analysis, comparing each bioreceptor response, was reported in [28] in PBS buffer showing that the cross-sensitivity between the proteins is quite marginal. This is justified by the fact that the measurement involves low-concentration detection, in line with the assumption that the wastewater samples contain a low amount of viral content and therefore the environmental refractive index surrounding the sensors remains approximately unaltered during the measurement, while biofunctionalized sensors provide a response due to the proteins binding in correspondence of the active surface [45].

3.3. Repeatability

The repeatability of the fabrication and interrogation of the SDI/FBG was assessed by exposing 5 sensors to proteins in a concentration ranging from 2.5 pM up to 400 nM, into wastewater samples. All sensors have been functionalized with A27 antibodies and perform simultaneous detection of the protein mixtures. The results are shown in Fig. 9, where the response of each sensor is compared. The responses at the highest protein concentrations range from 0.15 dB to 0.42 dB, while all sensors show a quite significant standard deviation. At the lowest concentration, we observe that four sensors have a detectable change

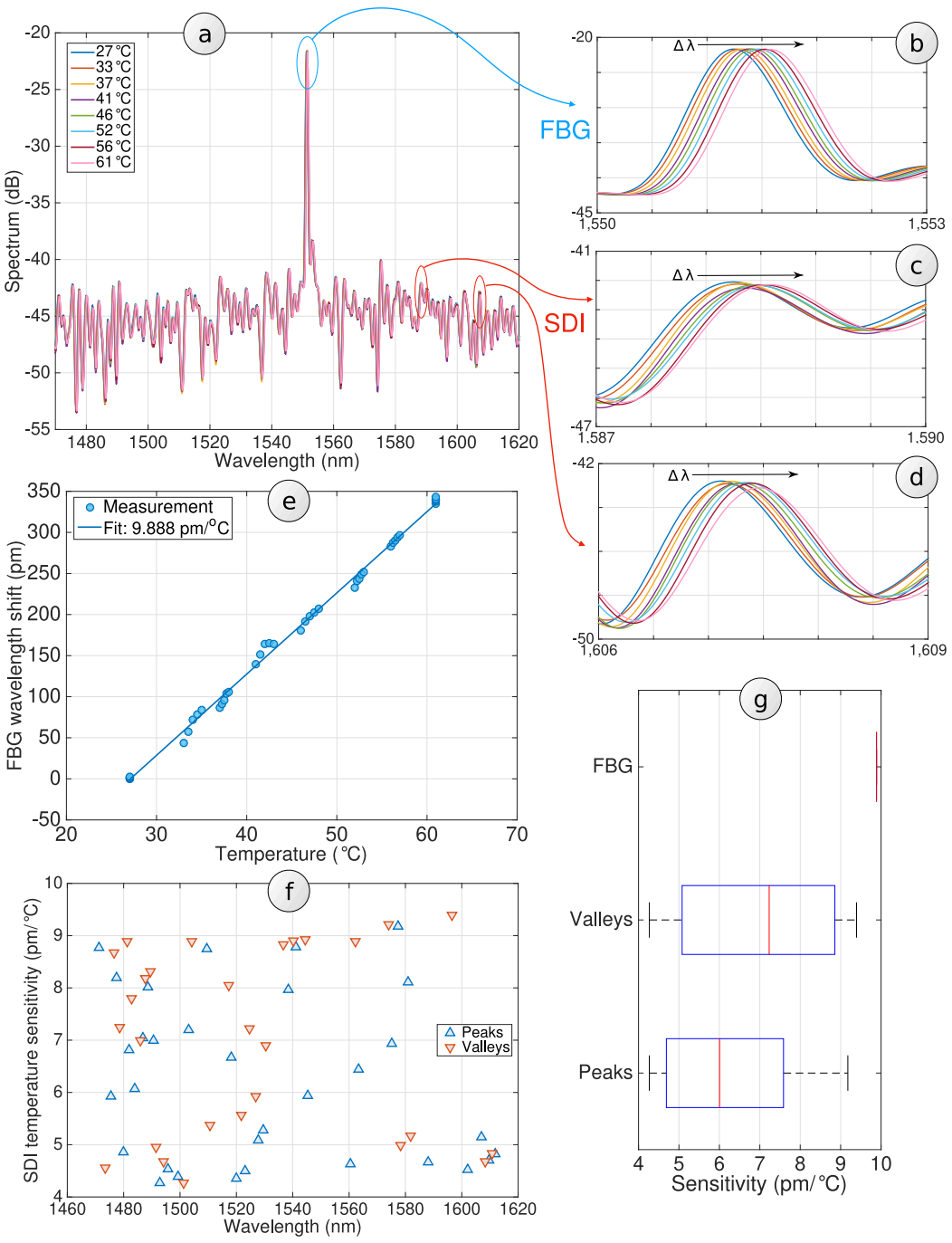

Fig. 6. Temperature sensitivity for the SDI/FBG probe. (a) The spectrum of a sensor evaluated at different temperature values. (b) Inset on the FBG wavelength shift. (c-d) Inset on two SDI spectral portions showing the wavelength shift of peaks. (e) Wavelength shift of the FBG with respect to temperature and evaluation of the thermal sensitivity. (f) Estimated temperature sensitivity for each peak/valley localized within the SDI spectrum. (g) Boxplot reproducing the thermal sensitivity for the SDI (peaks and valleys) compared to the FBG.

(0.06–0.13 dB) that is at least 3 times higher than the uncertainty of the interrogator, while one sensor has a negative response of −0.02 dB. Fig. 9(b) displays the repeatability band, which displays the average and standard deviation of the responses of the 5 sensors; the average response shows a quite linear trend with a slope of 0.0343 dB for each 10-fold increment of concentration ($R^2 = 0.93$), while the maximum of the standard deviation is ±0.07 dB.

3.4. Dynamic detection

In order to validate the real-time detection capabilities in wastewater samples that get progressively loaded onto the sensor surface, we performed experiments in which multiple detections were performed, changing the medium surrounding the sensor. Such experiments, reported in Fig. 10, demonstrate the capability of the sensors to undergo two detection cycles, performed by increasing the concentration of proteins in wastewater from 10 fM to 4 pM, at low concentration, changing the medium from wastewater to BSA, and then repeating the cycle, hence validating whether the SDI/FBG probes can function in multiple cycles. Two sensors were functionalized for this test, using L1 and A27 antibodies.

The spectral analysis, shown in Fig. 10(a-b) details how the spectrum

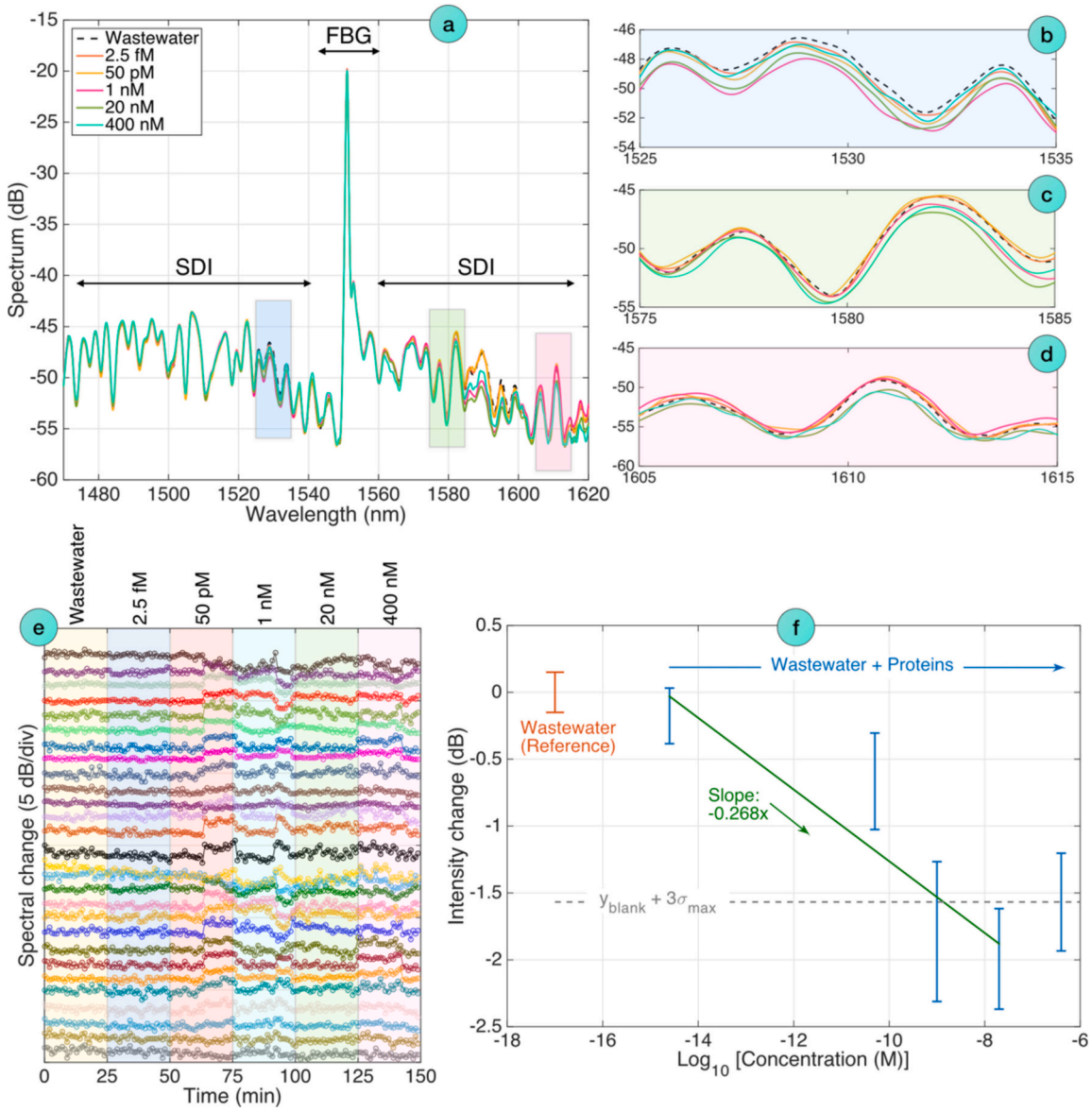

Fig. 7. Direct detection of vaccinia protein mixtures at various concentrations in wastewater, using a sensor biofunctionalized with anti-L1 antibodies. (a) The spectrum of the functionalized SDI/FBG biosensor at various concentrations, after 5 min of exposure; (b-d) Insets on spectral portions. (e) Temporal evolution of the intensity of each spectral valley after exposure of proteins at various concentrations. (f) Response of the L1-biosensor to the protein concentrations, visualizing the linear regression and detection limit; errorbars show ± standard deviation over 10 consecutive measurements.

evolves throughout the detection. The largest spectral changes occur, as expected, through the change of the medium. Since the proteins are detected at low concentrations, the spectral changes are limited throughout the detection cycles, but a larger change is observed when changing the surrounding medium. The sensorgram and response analysis shown in Fig. 10(c-d) shows that, in this dynamic detection context, the spectral changes that we observe in the first cycle of detection follow linear trends with a gentle slope of −0.0599 dB (L1) and − 0.0237 dB (A27) for each 10-fold protein concentration increment. The higher response for the L1-functionalized sensor (2.5 times higher than A27) is in agreement with the static acquisition data. The larger analyte change that we observed is in correspondence to the analyte change: this corresponds to a spectral change of −0.90 dB for the L1 sensor, and − 1.65 dB for A27, which strongly differentiates the surrounding RI changes from the small-scale analysis that involves the changes in the protein concentrations. The second cycle of detection still shows that the sensors have the capability of detecting protein changes, as the measurement slopes are estimated as +0.0724 dB (L1) and − 0.1529 dB (A27), both higher than in the first measurement round. We observe that the trend for the L1 protein appears to reverse the slope, and this is possibly due to the different RI surrounding the medium after the background medium change; this was observed in prior SDI demonstrations [25], where the RI sensitivity is either observed with negative or positive slope.

The dynamic analysis shows that, as expected, the background RI changes affect the sensor more than the protein detection, particularly at low concentrations, yet the sensors have still a sufficient resolution to detect through more than one cycle of exposure and over the resolution threshold of the interrogator. Since this measurement mimics a long-term exposure of the biosensors to wastewater samples that get continuously loaded onto the sensor, it is possible to confirm that the sensor has the capability of working at various environmental conditions and that the SDI/FBG cross-sensitivities are not affecting the measurement quality. As observed in Supplementary Figs. S4-S5, throughout the dynamic measurement cycles the residual spectral shifts observed by the FBG and the SDI are minimal (around 0.5 pm for the FBG and around

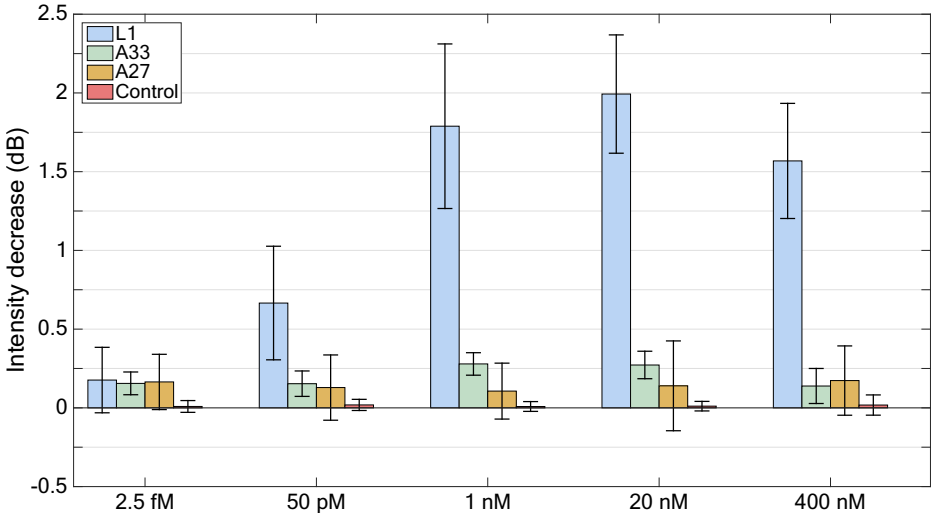

Fig. 8. Comparison of the response for L1, A33, and A27 biofunctionalized sensor, and a negative control sensor, performing direct detection of vaccinia proteins in a wastewater sample. The chart reports the average response (bars), and ± standard deviation (errorbars).

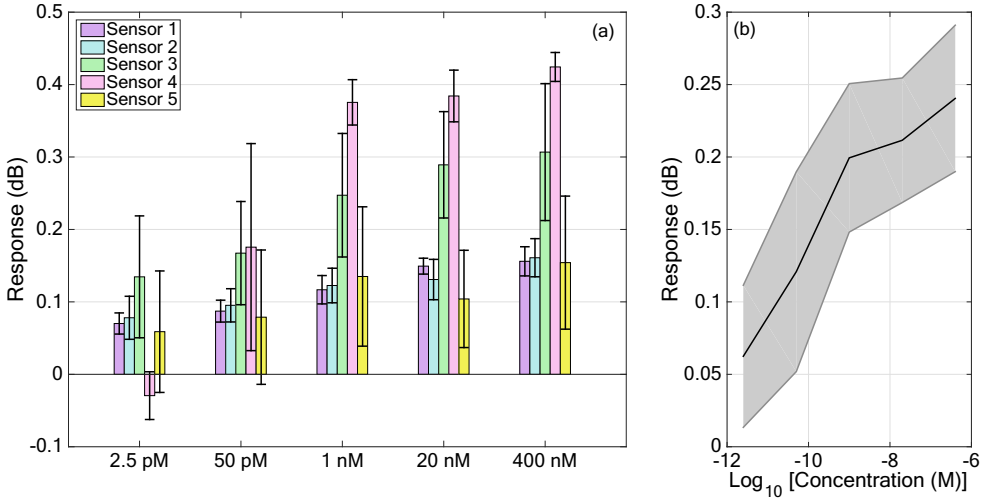

Fig. 9. Repeatability of the SDI/FBG probes for protein detection. (a) Response of 5 probes exposed to protein concentration changes (bars = average; errorbars = ± standard deviation). (b) The repeatability range showing the average and standard deviation of the output of the whole set of sensors.

0.1 pm for the SDI), which confirms that the temperature changes do not influence the biological detection since they correspond to ~0.05 °C of changes. Similarly, as the FBG is RI-insensitive, the fluctuations of the FBG spectra are small (<0.03 dB in correspondence to the surrounding medium changes).

4. Conclusions

In conclusion, we reported in this work the design of a sensing system based on fiber-optic SDI/FBG probes suitable for the continuous detection of viral threats in wastewater. The probe combines two sensing elements: i) a wide-band interferometer with random envelope, formed by a short section of enhanced backscattering fiber spliced to an SMF fiber, and the cleaved tip, which encodes refractive index changes by modulating the intensity of each spectral peak/valley with sensitivity up to 266.1 dB/RIU; ii) a narrowband FBG, which encodes a temperature variation (sensitivity 9.888 pm/°C) and allows compensating for thermal variations in the surrounding environment. The use of FBG gratings also makes the probes compatible with standard FBG interrogators, which have a lower cost and better multiplexing capabilities than distributed sensing hardware that was used in prior demonstrations [33].

As a case scenario, the probes have been functionalized for the detection of proteins expressed by vaccinia virus, which share a high sequence homology with smallpox proteins. Previous reports showed that sensors biofunctionalized with protein-binding antibodies exhibit similar patterns, both quantitatively and qualitatively, when exposed to protein concentration changes [28] and when performing the detection of vaccinia virus [33]. The sensors used in this work have been functionalized with antibodies specific for L1, A27, and A33, and were tested for dynamic changes of proteins through various concentrations.

The experimental results show that the SDI/FBG probes have good stability, a high specificity, and enable the capability to detect proteins at small concentrations. The system was first tested in a direct detection format, whereas proteins were continuously detected in ascending concentrations in the same sample of wastewater. The results show that the anti-L1-functionalized sensor yields a higher response, up to 1.99 dB intensity change and 9.1–11.3 times higher than sensors functionalized with antibodies specific for A33 and A27, respectively. The system has a capability for detection even at low concentrations, particularly with anti-L1 antibodies where a change of 0.18 dB is observed at 2.5 fM and 0.67 dB at 50 pM levels. Dynamic testing also was performed, mimicking

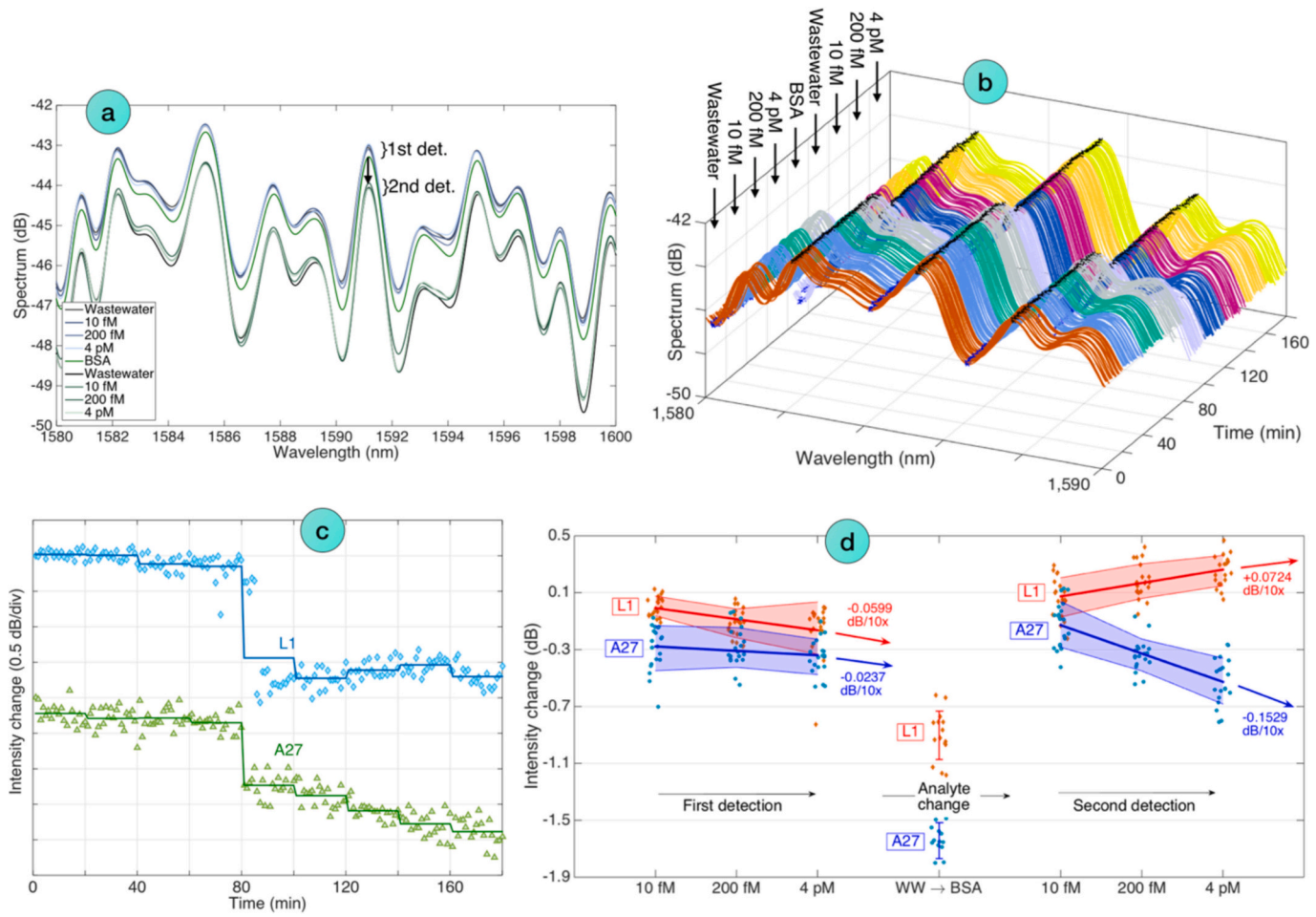

Fig. 10. Dynamic detection of wastewater samples, undergoing a continuous updating process. (a) Portion of the spectra of an L1-functionalized sensor after 5 min of each detection step. (b) Dynamic evolution of the SDI spectral portion through the measurement. (c) Sensorgrams showing the response of two sensors functionalized with L1 and A27 antibodies. (d) Analysis of the responses for L1 and A27 sensors throughout the detection cycle. Data points = experimental analysis; ranges = average and standard deviation over 20 consecutive measurements.

the systems designed for continuous collection and detection of wastewater samples; in this case, the system is capable of detecting protein concentrations (with sensitivity ranging from 0.024 dB to 0.153 dB for every 10-fold increment of concentration), and to detect with a larger change the variation of the surrounding analyte (0.90–1.65 dB).

The obtained results provide a first proof of concept for detection directly in wastewater samples, with the objective of moving towards detection of either processed wastewater samples, similar to the monitoring system deployed for the COVID-19 pandemic and used to correlate the detected viral titers to the number of viral infection cases [46], but also with the possibility of performing a direct detection into a wastewater sample that gets continuously updated [30]. While previous experimental reports showed very consistent trends in enriched PBS buffers [33], the operation in wastewater appears to have lower performances, both in terms of sensitivity and, even more noticeably, in terms of detection trends. Experiments show that results do not follow a log-polynomial pattern that matches previous works, but rather the detection trends are still non-monotonic across a wide range of concentrations. The obtained platform presented hereby is proven in the context of viral detection; however, exploiting the versatility of fiber optic biosensors in immunology and the format of label-free functionalization, it might be extended to detection of other biomolecules, such as in previously reported studies that report the detection of hormones [47,48], bacteria [49], and toxins [50].

For these reasons, we can conclude that the proof of concept presented in this work provides a first stepping stone over the use of fiber-optic dynamic sensors optimized for biosafety applications, directly into wastewater; the proposed system has therefore the functionality of a first-responder unit [51]. Future works will need to address the functionalization of the sensors, and their placement into reservoirs for a more accurate exposure of each device to viral threats, in order to optimize the detection of specific viral threats over a broad working range, resolving the concentration levels with higher precision; this will also involve handling the wastewater samples, possibly using pre-filtering and anti-fouling methods, in order to improve the measurement accuracy.

Funding

The research was funded through Nazarbayev University, under grants M2O-DISK (code: 20122022FD4134) and SMARTER (code: 091019CRP2117); the work was also supported by North Atlantic Treaty Organization (NATO) under the Science for Peace and Security program (grant G5486).

CRediT authorship contribution statement

Albina Abdossova: Writing – review & editing, Writing – original draft, Validation, Methodology, Conceptualization. **Aina Adilzhankyzy:** Writing – review & editing, Writing – original draft, Validation, Methodology, Conceptualization. **Kuanysh Seitkamal:** Writing – review & editing, Writing – original draft, Validation, Methodology,

Conceptualization. **Massimo Olivero:** Writing – review & editing, Investigation. **Guido Perrone:** Writing – review & editing, Investigation. **Wilfried Blanc:** Writing – review & editing, Resources, Investigation. **Luca Vangelista:** Writing – review & editing, Resources, Investigation, Funding acquisition. **Daniele Tosi:** Writing – review & editing, Writing – original draft, Funding acquisition, Formal analysis, Data curation, Conceptualization.

Declaration of competing interest

The authors declare that they have no known competing financial interests or personal relationships that could have appeared to influence the work reported in this paper.

Data availability

Data will be made available on request.

Appendix A. Supplementary data

Supplementary data to this article can be found online at https://doi.org/10.1016/j.sbsr.2024.100699.

References

[1] N. Boonham, et al., Methods in virus diagnostics: from ELISA to next generation sequencing, Virus Res. 186 (December) (2014) 20–31, https://doi.org/10.1016/j.virusres.2013.12.007.

[2] Y. Saylan, Ö. Erdem, S. Ünal, A. Denizli, An alternative medical diagnosis method: biosensors for virus detection, Biosensors 9 (2) (2019), https://doi.org/10.3390/bios9020065.

[3] N.K. Tran, S. Albahra, H. Rashidi, L. May, Innovations in infectious disease testing: Leveraging COVID-19 pandemic technologies for the future, Clin. Biochem. 117 (January 2022) (2023) 10–15, https://doi.org/10.1016/j.clinbiochem.2021.12.011.

[4] M.R. De Blasiis, C. Isonne, F. Turatto, E. Mazzalai, C. Marzuillo, C. De Vito, P. Villari, Attitudes and experiences towards the IMMUNI app among Sapienza university students: a pilot study, Eur. J. Pub. Health 32 (2022) 170–171.

[5] H. Zhu, et al., IoT PCR for pandemic disease detection and its spread monitoring, Sensors Actuators B Chem. 303 (September) (2019) 2020, https://doi.org/10.1016/j.snb.2019.127098.

[6] Y. Dong, Y.D. Yao, IoT platform for covid-19 prevention and control: a survey, IEEE Access 9 (2021) 49929–49941, https://doi.org/10.1109/ACCESS.2021.3068276.

[7] C.C. Lai, C.K. Hsu, M.Y. Yen, P.I. Lee, W.C. Ko, P.R. Hsueh, Monkeypox: an emerging global threat during the COVID-19 pandemic, J. Microbiol. Immunol. Infect. 55 (5) (2022) 787–794, https://doi.org/10.1016/j.jmii.2022.07.004.

[8] R.S. Noyce, S. Lederman, D.H. Evans, Construction of an infectious horsepox virus vaccine from chemically synthesized DNA fragments, PLoS One 13 (1) (2018) 1–16, https://doi.org/10.1371/journal.pone.0188453.

[9] R.S. Noyce, D.H. Evans, Synthetic horsepox viruses and the continuing debate about dual use research, PLoS Pathog. 14 (10) (2018) 1–5, https://doi.org/10.1371/journal.ppat.1007025.

[10] M. Madadelahi, R. Agarwal, S.O. Martinez-Chapa, M.J. Madou, A roadmap to high-speed polymerase chain reaction (PCR): COVID-19 as a technology accelerator, Biosens. Bioelectron. 246 (November 2023) (2024) 115830, https://doi.org/10.1016/j.bios.2023.115830.

[11] A. Tahamtan, A. Ardebili, Real-time RT-PCR in COVID-19 detection: issues affecting the results, Expert. Rev. Mol. Diagn. 20 (5) (2020) 453–454, https://doi.org/10.1080/14737159.2020.1757437.

[12] M. Bellon, et al., Cerebrospinal fluid features in severe acute respiratory syndrome coronavirus 2 (SARS-CoV-2) reverse transcription polymerase chain reaction (RT-PCR) positive patients, Clin. Infect. Dis. 73 (9) (2021) E3102–E3105, https://doi.org/10.1093/cid/ciaa1165.

[13] T. Lewis, E. Giroux, M. Jovic, S. Martic-Milne, Localized surface plasmon resonance aptasensor for selective detection of SARS-CoV-2 S1 protein, Analyst 146 (23) (2021) 7207–7217, https://doi.org/10.1039/d1an01458g.

[14] Y. Zheng, S. Bian, J. Sun, L. Wen, G. Rong, M. Sawan, Label-free LSPR-vertical microcavity biosensor for on-site SARS-CoV-2 detection, Biosensors 12 (3) (2022) 1–13, https://doi.org/10.3390/bios12030151.

[15] Z. Zhang, et al., A novel enhanced substrate for label-free detection of SARS-CoV-2 based on surface-enhanced Raman scattering, Sensors Actuators B Chem. 359 (January) (2022) 131568, https://doi.org/10.1016/j.snb.2022.131568.

[16] N. Cennamo, et al., SARS-CoV-2 spike protein detection through a plasmonic D-shaped plastic optical fiber aptasensor, Talanta 233 (May) (2021) 122532, https://doi.org/10.1016/j.talanta.2021.122532.

[17] A. Bekmurzayeva, M. Nurlankyzy, A. Abdossova, Z. Myrkhiyeva, D. Tosi, All-fiber label-free optical fiber biosensors: from modern technologies to current applications [invited], Biomed. Opt. Express 15 (3) (2024) 1453, https://doi.org/10.1364/boe.515563.

[18] D. Tosi, Review and analysis of peak tracking techniques for fiber bragg grating sensors, Sensors (Switzerland) 17 (10) (2017), https://doi.org/10.3390/s17102368.

[19] A. Beisenova, et al., Distributed sensing network enabled by high-scattering MgO-doped optical fibers for 3d temperature monitoring of thermal ablation in liver phantom, Sensors (Switzerland) 21 (3) (2021) 1–10, https://doi.org/10.3390/s21030828.

[20] I. Ashry, et al., A review of distributed Fiber-optic sensing in the oil and gas industry, J. Lightwave Technol. 40 (5) (2022) 1407–1431, https://doi.org/10.1109/JLT.2021.3135653.

[21] Y. Choi, S.H. Abbas, J.R. Lee, Aircraft integrated structural health monitoring using lasers, piezoelectricity, and fiber optics, Meas. J. Int. Meas. Confed. 125 (April) (2018) 294–302, https://doi.org/10.1016/j.measurement.2018.04.067.

[22] A. Bogler, et al., Rethinking wastewater risks and monitoring in light of the COVID-19 pandemic, Nat. Sustain. 3 (12) (2020) 981–990, https://doi.org/10.1038/s41893-020-00605-2.

[23] D.L. Jones, et al., Suitability of aircraft wastewater for pathogen detection and public health surveillance, Sci. Total Environ. 856 (September 2022) (2023) 159162, https://doi.org/10.1016/j.scitotenv.2022.159162.

[24] A.W. Gomez, Z. Myrkhiyeva, M. Tilegen, T.T. Pham, A. Bekmurzayeva, D. Tosi, Optical Fiber ball resonator biosensor as a platform for detection of diabetic retinopathy biomarkers in tears, IEEE Sensors J. 24 (7) (2024) 11127–11135, https://doi.org/10.1109/JSEN.2024.3363219.

[25] S. Kazhiyev, A. Abdossova, D. Moldabay, A. Rakhimbekova, W. Blanc, D. Tosi, Semi-distributed interferometers fiber-optic sensors for high-sensitivity refractive index detection: design and sensitivity analysis, Meas. J. Int. Meas. Confed. 220 (July) (2023) 113327, https://doi.org/10.1016/j.measurement.2023.113327.

[26] A. Rakhimbekova, et al., Fiber-optic semi-distributed Fabry-Perot interferometer for low-limit label-free detection of CCL5 cancer biomarker, Opt. Laser Technol. 168 (May 2023) (2024) 109953, https://doi.org/10.1016/j.optlastec.2023.109953.

[27] K. Karipbayeva, W. Blanc, D. Tosi, Optical Fiber semi-distributed interferometer assisted by an FBG for Thermorefractometry and sweat sensing, IEEE Sensors J. 23 (13) (2023) 14161–14166, https://doi.org/10.1109/JSEN.2023.3277004.

[28] K. Seitkamal, et al., Proof of principle for a sensitive, real time and label-free detection of poxviruses using optical fiber biosensors, Optik (Stuttg). 288 (May) (2023) 1–12, https://doi.org/10.1016/j.ijleo.2023.171195.

[29] C. Wang, M. Liu, Z. Wang, S. Li, Y. Deng, N. He, Point-of-care diagnostics for infectious diseases: from methods to devices, Nano Today 37 (2021) 101092, https://doi.org/10.1016/j.nantod.2021.101092.

[30] D. Barceló, Wastewater-Based Epidemiology to monitor COVID-19 outbreak: Present and future diagnostic methods to be in your radar, Case Stud. Chem. Environ. Eng. 2 (July) (2020), https://doi.org/10.1016/j.cscee.2020.100042.

[31] C.G. Daughton, Wastewater surveillance for population-wide Covid-19: the present and future, Sci. Total Environ. 736 (2020) 139631, https://doi.org/10.1016/j.scitotenv.2020.139631.

[32] F. Wu, et al., SARS-CoV-2 RNA concentrations in wastewater foreshadow dynamics and clinical presentation of new COVID-19 cases, Sci. Total Environ. 805 (August 2021) (2022) 150121, https://doi.org/10.1016/j.scitotenv.2021.150121.

[33] A. Rakhimbekova, et al., Rapid detection of vaccinia virus using biofunctionalized fiber-optic ball-tip biosensors, Sci. Rep. 13 (1) (2023) 1–11, https://doi.org/10.1038/s41598-023-44926-6.

[34] A. Bekmurzayeva, et al., Ultra-wide, attomolar-level limit detection of CD44 biomarker with a silanized optical fiber biosensor, Biosens. Bioelectron. 208 (December 2021) (2022) 114217, https://doi.org/10.1016/j.bios.2022.114217.

[35] V.A. Tang, et al., Single-particle characterization of oncolytic vaccinia virus by flow virometry, Vaccine 34 (42) (2016) 5082–5089, https://doi.org/10.1016/j.vaccine.2016.08.074.

[36] International Organization for Standardization (ISO), ISO 11733:2004 – Water Quality—Determination of the Elimination and Biodegradability of Organic Compounds in an Aqueous Medium—Activated Sludge Simulation Test [Online]. Available: https://www.iso.org/standard/34416.html, 2004.

[37] D. Tosi, C. Molardi, M. Sypabekova, W. Blanc, Enhanced backscattering optical Fiber distributed sensors: tutorial and review, IEEE Sensors J. 21 (11) (2021) 12667–12678, https://doi.org/10.1109/JSEN.2020.3010572.

[38] R. Gassino, G. Perrone, A. Vallan, Temperature monitoring with fiber bragg grating sensors in nonuniform conditions, IEEE Trans. Instrum. Meas. 69 (4) (2020) 1336–1343, https://doi.org/10.1109/TIM.2019.2909943.

[39] D.L.O. Presti, et al., Fiber Bragg gratings for medical applications and future challenges: a review, IEEE Access 8 (2020) 156863–156888.

[40] A. Beccaria, et al., Temperature monitoring of tumor hyperthermal treatments with optical fibers: comparison of distributed and quasi-distributed techniques, Opt. Fiber Technol. 60 (June) (2020) 102340, https://doi.org/10.1016/j.yofte.2020.102340.

[41] "Water Resources Research - 2018 - Shanafield - Fiber-Optic Sensing for Environmental Applications Where We Have Come From.pdf." n.d.

[42] J.K. Sahota, N. Gupta, D. Dhawan, Fiber Bragg grating sensors for monitoring of physical parameters: a comprehensive review, Opt. Eng. 59 (06) (2020) 1, https://doi.org/10.1117/1.oe.59.6.060901.

[43] M. Sypabekova, A. Amantayeva, L. Vangelista, Á. González-Vila, C. Caucheteur, D. Tosi, Ultralow limit detection of soluble HER2 biomarker in serum with a Fiber-optic ball-tip resonator assisted by a tilted FBG, ACS Meas. Sci. Au 2 (4) (2022) 309–316, https://doi.org/10.1021/acsmeasuresciau.2c00008.

[44] A. Bekmurzayeva, et al., Label-free fiber-optic spherical tip biosensor to enable picomolar-level detection of CD44 protein, Sci. Rep. 11 (1) (2021) 1–13, https://doi.org/10.1038/s41598-021-99099-x.
[45] F. Chiavaioli, C.A.J. Gouveia, P.A.S. Jorge, F. Baldini, Towards a uniform metrological assessment of grating-based optical fiber sensors: from refractometers to biosensors, Biosensors 7 (2) (2017), https://doi.org/10.3390/bios7020023.
[46] C. Schmidt, Watcher in the wastewater, Nat. Biotechnol. 38 (8) (2020) 917–920, https://doi.org/10.1038/s41587-020-0620-2.
[47] H.C. Gomes, et al., Laser-induced graphene-based Fabry-Pérot cavity label-free immunosensors for the quantification of cortisol, Sensors Actuat. Reports 7 (December) (2023) 2024, https://doi.org/10.1016/j.snr.2024.100186.
[48] X. Liu, et al., SFFO cortisol biosensor: highly sensitive S-flex Fiber optic Plasmonic biosensor for label-free cortisol detection, IEEE Sensors J. 24 (2) (2024) 1494–1501, https://doi.org/10.1109/JSEN.2023.3336414.
[49] C. Gu, et al., Development of W-type four-Core Fiber-based WaveFlex sensor for enhanced detection of Shigella Sonnei Bacteria using engineered nanomaterials, J. Lightwave Technol. 42 (14) (2024) 5055–5067, https://doi.org/10.1109/JLT.2024.3379290.
[50] T. de Andrade Silva, et al., Plasmonic immunosensors based on spoon-shaped waveguides for fast and on-site ultra-low detection of ochratoxin A in coffee samples, Talanta 271 (October 2023) (2024) 125648, https://doi.org/10.1016/j.talanta.2024.125648.
[51] T. Joseph, Management system approach for addressing biosafety and biosecurity of emerging pathogens in a biosafety Level-3 Core Facility, Appl. Biosaf. 26 (4) (2021) 210–220, https://doi.org/10.1089/apb.2021.0007.